

## Static magnetic fields enhance lipid order in native plant plasma membrane

Cite this: *Soft Matter*, 2013, **9**, 6804

Danny Poinapen,<sup>†abc</sup> Laura Toppozini,<sup>†\*e</sup> Hannah Dies,<sup>d</sup> Daniel C. W. Brown<sup>af</sup> and Maikel C. Rheinstädter<sup>\*deg</sup>

We studied molecular order in native plant plasma membranes in the presence of static magnetic fields. Plasma membranes of seeds of the tomato plant were purified, extracted, and applied to a silicon substrate in a buffer suspension and their molecular structure was studied using X-ray diffraction. We observed correlation peaks that we assigned to the lipid and protein components of the plasma membrane. Two field strengths were available:  $B = 0.126$  T and  $B = 0.208$  T. While magnetic fields had no observable effect on protein structure, enhanced lipid order was observed, leading to an increase in the gel components and a decrease in the fluid component of the lipids.

Received 3rd February 2013

Accepted 1st April 2013

DOI: 10.1039/c3sm50355k

www.rsc.org/softmatter

Magnetic fields are known to interact with biological systems in various ways. Animals, such as pigeons and certain ants, use magnetic fields for orientation.<sup>1–4</sup> Magnetic bacteria move along the direction of an external applied  $\vec{B}$  field.<sup>5,6</sup> Biological systems show a weak diamagnetism, which was used to levitate live animals, such as a grasshopper, mouse and frog.<sup>7</sup> Static magnetic fields of 0.2 T routinely generated by a magnetic resonance tomograph were found to induce alterations on human skin fibroblasts.<sup>8</sup>

In plants, more specifically in their seeds, enhanced germination was reported after exposure to magnetic fields but to date the underlying mechanism has not been resolved.<sup>9–11</sup> The germination process starts by water uptake and is accompanied by electrolyte leakage due to seed membrane impairment.<sup>12</sup> Because it was observed that seed exposure to static magnetic fields reduced seed electrolyte leakage during imbibition, it was deduced that static magnetic fields could influence seed membranes and likely the plasma membrane.

We studied molecular structure of plant plasma membrane using X-ray diffraction, as sketched in Fig. 1. Signals related to  $\alpha$ -helical structures in the proteins and gel and fluid lipid tail

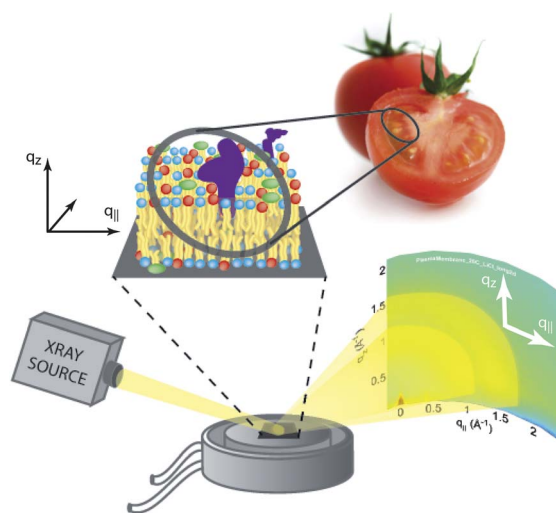


**Fig. 1** Schematic diagram of the instrumental setup for the X-ray experiments. The purified plasma membranes of tomato seeds were placed in a storage buffer and deposited on 2 cm × 2 cm silicon wafers. The molecular structure of the membranes was determined from 2-dimensional intensity maps. By placing the wafers on top of permanent magnets, the effect of external magnetic fields on protein and lipid structure was studied.

<sup>a</sup>Department of Biology, University of Western Ontario, London, ON, Canada. E-mail: dpoinapen@gmail.com

<sup>b</sup>Southern Crop Protection and Food Research Centre, Agriculture and Agri-Food Canada, London, ON, Canada

<sup>c</sup>Department of Physics, University of Mauritius, Réduit, Mauritius

<sup>d</sup>Department of Physics and Astronomy, McMaster University, Hamilton, ON, Canada. E-mail: toppozl@mcmaster.ca; rheinstadter@mcmaster.ca

<sup>e</sup>Origins Institute, McMaster University, Hamilton, ON, Canada

<sup>f</sup>Canadian Centre for Agri-Food Research in Health and Medicine, St. Boniface Hospital Research Centre, Winnipeg, MB, Canada

<sup>g</sup>Canadian Neutron Beam Centre, National Research Council Canada, Chalk River, ON, Canada

† These authors have contributed equally to this work.

structures in the membrane were observed. By studying the intensity of the corresponding signals as function of applied magnetic field, we observed that static magnetic fields enhance lipid order in native plasma membranes.

## Materials and methods

### Preparation of plasma membrane

Tomato seeds (*Solanum lycopersicum* var Heinz H1439) were used for plasma membrane isolation and purification. All steps were carried out at 4 °C or on ice. 40 g of seeds were frozen with

liquid nitrogen and immediately pulverized in a steel ball mill at maximum speed for  $4 \times 50$  s. The fine seed materials were immediately added to 100 mL of extraction buffer<sup>13,14</sup> containing 70 mM Trizma base (pH 8.0), 330 mM sucrose, 5 mM EDTA, 10 mM KCl, 3 mM MgCl<sub>2</sub>, 0.6% PVP, 0.2% casein, 2 tablets (per 50 mL buffer) of protein inhibitor cocktail, 5 mM DTT (added freshly), and 15 mM  $\beta$ -mercaptoethanol (added freshly). The homogenate was thoroughly mixed and then filtered through two layers of nylon cloth (250  $\mu$ m) to remove debris.

The filtrate was first centrifuged at 10 000g to remove a maximum amount of starch and other suspensions.<sup>15</sup> The supernatant was further centrifuged at 20 000g to precipitate remaining starchy particles. The supernatant was collected and further centrifuged at 200 000g for 45 minutes to collect microsomal fractions. The pelleted membrane vesicles were taken up in 9 mL resuspension buffer containing: 5 mM Trizma (pH 7.5), 330 mM sucrose, 2 tablets (per 50 mL buffer) of protein inhibitor cocktail, and 1 mM DTT (added fresh) made up to 9 mL. A plasma membrane enriched fraction was obtained by adding the 9 mL microsomal fraction to 27 g two-phase polymer partitioning containing 6.4% (w/w) dextran T-500; 6.4% (w/w) PEG-3350; 5 mM phosphate buffer (pH 7.8), 5 mM KCl, 300 mM sucrose (topped up to 27 grams with ultra pure water). The system was vigorously shaken 20 times and then centrifuged at 2000g for 10 minutes. Purification of the plasma membrane from the initial upper phase (PEG layer) was obtained by adding it to a fresh lower phase (dextran layer), while the initial lower phase is added to a fresh upper phase. These phases were thoroughly mixed and centrifuged at 2000g for 10 minutes (this procedure was repeated 3 times each time using fresh upper and lower phases). These upper phases were collect and diluted in 60 mL washing buffer (10 mM Trizma base (pH 8.3), 10 mM boric acid, 300 mM sucrose, 9 mM KCl, 5 mM EDTA, 50 mM NaF) and pelleted at 200 000g for 35 minutes. Purified plasma membrane pellets were then resuspended in 1 mL membrane buffer (10 mM Trizma base (pH 8.3), 10 mM boric acid, 300 mM sucrose, 9 mM KCl, 5 mM EDTA, 50 mM NaF, 1 tablet of protein inhibitor cocktail (per 25 mL), and 5 mM DTT) and stored at  $-80$  °C.

The purity of the plasma membranes was tested before the experiments. For the protein gel blot analysis, as shown in Fig. 2, the protein concentration was first quantified according to the Bradford method<sup>16</sup> using bovine serum albumin (BSA) as standard. 3.3  $\mu$ g of total protein extract as well as equal amounts of the microsomal fraction, and purified plasma membrane were resolved on 8% SDS-PAGE and electro blotted on PVDF membranes. The membranes were blotted in TBS-T with 5% nonfat milk at room temperature for 1 hour. The blot was then incubated with the primary antibody H + ATPase (Agriser, Sweden) in blocking solution at 1 : 2500 at 4 °C overnight. The primary Ab was washed off using 0.5% blocking solution before being probed with Goat anti-rabbit HRP-conjugate secondary antibody (Biorad, Canada) at 1 : 10 000 dilutions in 0.5% blocking solution for 1 hour. After washing in TBST, Amersham ECL plus detection reagents was added (Ge, Healthcare, USA) to the membrane and allowed to develop on photographic film.

The plasma membrane purity was further quantified by assaying ATPase activity with and without inhibitors according

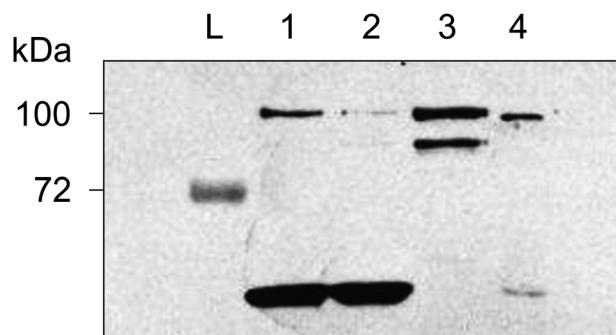


**Fig. 2** Expression levels of plasma membrane biomarker H + ATPase (100 kDa) in protein blots at different stages from extraction up to purification. (L) Protein stained ladder marker; (1) total protein after centrifuging at 10 000g; (2) total protein after centrifugation at 20 000g; (3) microsomal fraction; and (4) purified plasma membrane fraction. Protein samples in lanes 1, 2, and 3 were reduced (in sample loading buffer containing  $\beta$ -mercaptoethanol) at 95 °C for 5 minutes. The plasma membrane sample in lane 4 was non-reduced ( $\beta$ -mercaptoethanol omitted in the sample loading buffer) at 50 °C for 60 minutes.

to a modified method.<sup>17</sup> Vanadate-inhibited ATPase is a plasma membrane marker while KNO<sub>3</sub> and NaN<sub>3</sub> were used to check for contamination by the tonoplasts and mitochondria, respectively. 2  $\mu$ g of plasma membrane sample was added to the reaction mixture containing 50 mM MOPS-Tris (pH 7.0), 50 mM KCl, 2 mM DTT, 0.1 mM EGTA and 12 mM ATP with and without ATPase inhibitors (0.1 mM NaVO, 50 mM KNO<sub>3</sub>, and 10 mM NaN<sub>3</sub>). 10  $\mu$ L (2  $\mu$ g) plasma membrane was added to 30  $\mu$ L of reaction mixture with and without inhibitors for the microassay. In the same plate 60  $\mu$ L of phosphate (Pi) solution (0, 3, 6, 15, 30, 60, 90 and 120 nmol) used to generate standard curve, and 30  $\mu$ L of 10% SDS added to 40  $\mu$ L reaction mixture (for background subtraction) in separate wells. The plate was incubated at 37 °C for 3 minutes. The reaction was started by adding 20  $\mu$ L ATP to the wells (except to the phosphate standard wells) for 30 minutes incubated at 37 °C. The reaction was stopped by adding 30  $\mu$ L of 10% SDS. 200  $\mu$ L of freshly prepared colour reagent (35 mM ammonium molybdate/15 mM zinc acetate in 10% ascorbic acid (pH 5)) was added to all wells and incubated at 37 °C for 20 minutes for colour to develop, after which absorbance was measured at 750 nm. ATPase activities was calculated after background subtraction according to the generated phosphate standard curve and expressed as nmol Pi per min per  $\mu$ g protein.

As listed in Table 1, vanadate resulted in 94.6% inhibition, KNO<sub>3</sub> and NaN<sub>3</sub> in 8.38% and 4.33% inhibition, respectively, indicating a high purity of the plasma membrane samples and a very low level of contamination by tonoplast and mitochondria. The structure of the plasma membrane complexes was determined from the X-ray experiments below.

#### X-ray sample preparation

100 mm diameter, 300  $\mu$ m thick single-side polished silicon (100) wafers were laser cut into  $2 \times 2$  cm<sup>2</sup> chips. The silicon substrates were cleaned in a piranha acid solution made of 98% concentrated H<sub>2</sub>SO<sub>4</sub> and 30% concentrated H<sub>2</sub>O<sub>2</sub> at a ratio of 3 : 1 by volume. Wafers were placed in this solution, covered

**Table 1** ATPase activity of the purified plasma membrane with and without vanadate, nitrate, and azide inhibitors to estimate purity of the plasma membrane and presence of tonoplasts as well as mitochondria, respectively. Values represent mean  $\pm$  S.E.,  $n = 4$

Plasma membrane fraction	ATPase activity, nmol Pi per min per $\mu$ g protein	ATPase sensitivity (%), w.r.t. absence of inhibitors
Without inhibitors	$0.167 \pm 0.025$	
+Na <sub>3</sub> VO <sub>4</sub>	$0.009 \pm 0.002$	94.6
+KNO <sub>3</sub>	$0.153 \pm 0.004$	8.38
+NaN <sub>3</sub>	$0.160 \pm 0.001$	4.33

with parafilm and heated to 298 K for 30 minutes. This treatment removed all organic contamination and left the substrates in a hydrophilic state. The purified plasma membranes were applied to the substrate and bathed in a storage buffer solution containing sucrose. 500  $\mu$ L of the plasma membrane solution was applied onto each wafer. The wafers were then slowly dried in a desiccator at 97.6% RH under a K<sub>2</sub>SO<sub>4</sub> salt solution for 3 days and 85.1% RH under a KCl salt solution for another 7 days until a dry, uniform film of about 20  $\mu$ m thickness had formed. The wafers were uniformly covered and the film was stable over a period of several months, with no sign of de-wetting under all conditions applied.

Prior to the X-ray experiments, the sample was placed in a desiccator with a beaker of ultra-pure water and allowed to hydrate for 24 hours. During this time the film took up water and transformed into a fluid state. After 24 hours the film looked completely wet, without any visible internal structure. The re-hydration ensured the erasure of any “memory” of previous experiments or handling.

After this hydration period, the water beaker was removed and replaced with a saturated solution of lithium chloride (LiCl) for a period of at least 12 hours to completely dry the film. The sample was then mounted inside a hydration chamber on the X-ray machine. Different salt solutions were used to achieve relative humidities between  $\sim$ 11% and  $\sim$ 75% during the measurement, as listed in Table 2. A typical X-ray measurement took  $\sim$ 27 hours including a waiting loop of 2 hours to allow the membranes to equilibrate to the humidity level. All measurements were conducted at a temperature of  $T = 20$  °C. In experiments where magnets were used, the silicon chip was placed atop the south-facing side of the magnet(s) and was in this configuration during hydration, drying and X-ray measurement.

**Table 2** Saturated salt solutions and corresponding relative humidities used in this experiment

Saturated salt solution	Relative humidity RH at 20 °C (%)
LiCl	$11.3 \pm 0.4$
KOAc	$23.1 \pm 0.3$
K <sub>2</sub> CO <sub>3</sub>	$43.2 \pm 0.3$
NaCl	$75.5 \pm 0.1$

## Magnetic fields

Magnetic fields were generated by rare earth permanent magnets. The silicon substrates were directly placed onto the surface of  $\sim$ 2.5 cm  $\times$  2.5 cm  $\times$  0.2 cm neodymium magnets such that the South Pole was always in contact with the sample. Two magnets were mounted directly on top of each other to create a stronger field. Field strength and field geometry were measured with a high resolution Gauss meter at the sample position. The Hall probe was flat with a thickness of  $\sim$ 300  $\mu$ m, comparable to the silicon wafers such that the measured fields represent the fields at the plasma membrane position in the X-ray experiment. Fig. 3 depicts the magnetic field component perpendicular to the surface of the magnet,  $B_{\perp}$ , for one and two magnets. In the region of the sample (the central 2 cm  $\times$  2 cm) the average magnetic fields were measured to be 125.96 mT  $\pm$  46.35 mT for one magnet and 208.21 mT  $\pm$  38.90 mT for two magnets. Because the sample wafers were significantly smaller than the magnets and covered the centre area of the magnets, only, a relatively uniform field distribution was achieved.

## X-ray scattering experiment

X-ray scattering data was obtained using the Biological Large Angle Diffraction Experiment (BLADE) in the Laboratory for Membrane and Protein Dynamics at McMaster University. BLADE uses a 9 kW (45 kV, 200 mA) CuK $\alpha$  rotating anode at a wavelength of 1.5418 Å. Both source and detector are mounted on movable arms such that the sample stays horizontal during the measurements.<sup>18,19</sup> Multi-layer focussing optics provided a high intensity beam with monochromatic X-ray intensities up to

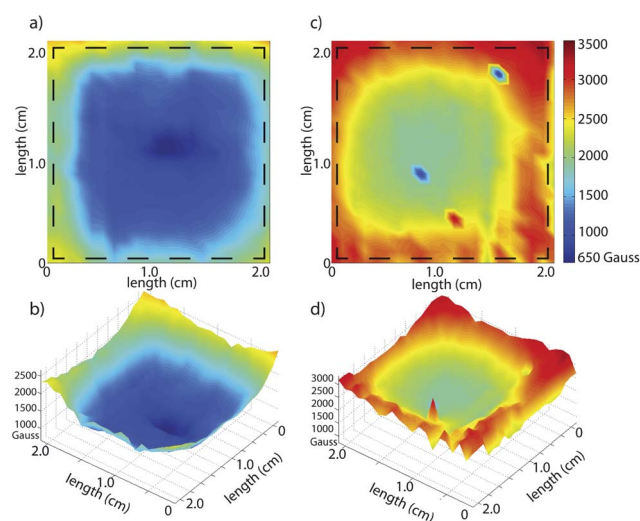


**Fig. 3** Rare earth neodymium magnets were used to create magnetic fields. Each magnet was 2.5 cm  $\times$  2.5 cm  $\times$  0.2 cm, the South Pole was always in contact with the sample. The magnetic field perpendicular to the surface was measured using a high-precision Gauss meter (GM-1-ST, AlphaLab Inc., USA); a total of 625 measurements were compiled for each magnet. Only the centre area of 2.1 cm  $\times$  2.1 cm is shown. The black dotted line depicts the outline of the 2 cm  $\times$  2 cm sample wafer. (a) Mapping of the magnetic field for one-magnet exposures and (b) topological map. (c) Mapping for the two-magnet exposures and (d) topological data. Average magnetic fields were determined to be 125.96 mT  $\pm$  46.35 mT and 208.21 mT  $\pm$  38.90 mT for one- and two-magnets, respectively.

$10^{10}$  photons per  $\text{mm}^2$  per s. This high intensity is a prerequisite to make small signals from proteins and lipids in the plasma membrane accessible. Data were obtained in reflection geometry using a collimated X-ray beam. A sketch of the scattering geometry is shown in Fig. 1. The result of such an X-ray experiment was a 2-dimensional intensity map of a large area ( $0.03 \text{ \AA}^{-1} < q_z < 2 \text{ \AA}^{-1}$  and  $0 \text{ \AA}^{-1} < q_{\parallel} < 2.5 \text{ \AA}^{-1}$ ) of the reciprocal space, as sketched in Fig. 1.  $q_z$  denotes the momentum transfer perpendicular to the silicon wafer,  $q_{\parallel}$  is the momentum transfer parallel to the wafer. The scattering vectors are related to real space distances by  $d = 2\pi/(q_z, q_{\parallel})$  such that the experiment covered length scales from  $\sim 3$  to  $150 \text{ \AA}$ , covering typical inter- and intra-lipid, and protein distances. The experiment was, therefore, sensitive to changes in the lipid and protein structure and conformational changes inside lipids and proteins.<sup>18,20,21</sup>

## Results

Fig. 4 shows typical X-ray data for plasma membrane in buffer and a pure buffer sample. The scattered intensity was distributed

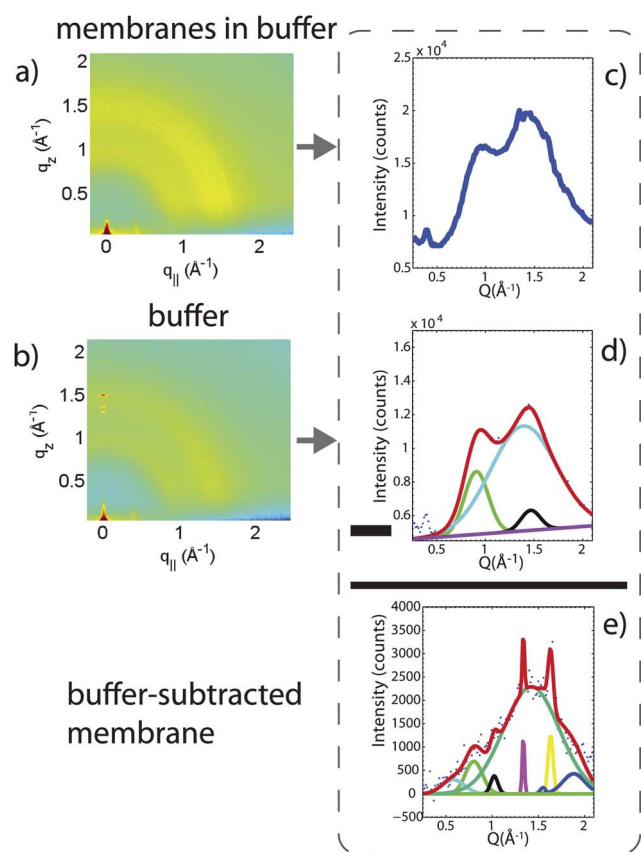


**Fig. 4** The results of the X-ray experiments are 2-dimensional intensity plots. Scattered intensity was found to be distributed in isotropic bands around the origin, indicative of a distribution of membrane orientations. (a) Two-dimensional intensity plot of plasma membrane in buffer solution on a Si wafer. (b) Two-dimensional intensity plot of the buffer solution on a Si wafer. The intensities were integrated over arcs from 0 to  $85.5^\circ$ , as shown in (c) and (d) for samples with and without plasma membrane, respectively. (e) Scans of plasma membranes in buffer were integrated and buffer-only sample integrations were subtracted. The subtracted data show a series of well developed correlation peaks, which can be assigned to the different molecular components.

over uniform rings about the origin. If the membranes aligned parallel to the silicon surface, the scattering should show a distinct intensity maximum along the in-plane axis,  $q_{\parallel}$ , as often reported in the literature.<sup>18,20,22</sup> Multi lamellar membranes are known to show a series of Bragg reflections along the out-of-plane axis,  $q_z$ , as a result of their periodic stacking. The absence of these features is indicative that the samples consist of single-membrane patches of plasma membrane, which are randomly oriented in the film on the substrate.

The 2-dimensional intensity maps of the buffer show two broad bands of intensity at  $Q$  values of  $\sim 1 \text{ \AA}^{-1}$  and  $\sim 1.5 \text{ \AA}^{-1}$  ( $Q = \sqrt{q_z^2 + q_{\parallel}^2}$ ), as shown in Fig. 4(b). Two additional sharper rings are observed at  $Q$  positions of  $\sim 1.4 \text{ \AA}^{-1}$  and  $\sim 1.6 \text{ \AA}^{-1}$  in the presence of plasma membrane in the film, as shown in Fig. 4(a).

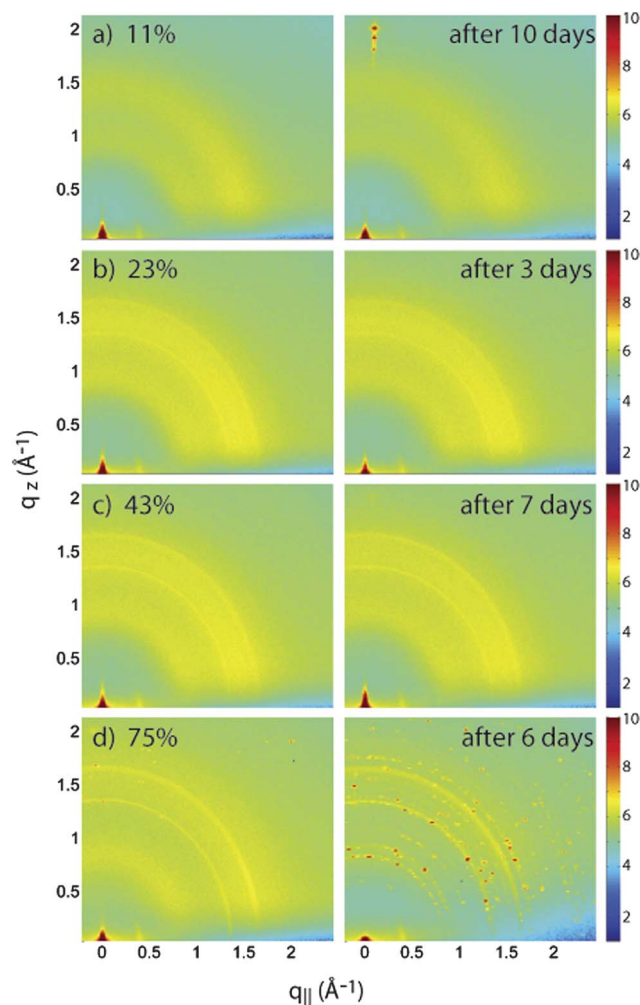


**Fig. 5** Stability of the plasma membrane structure over time while exposed to four relative humidities (RH). (a) LiCl provides an 11.3% RH environment which resists structural change for at least 10 days. (b) KOAc provides a 23.1% RH. Membrane structure changed over the total scanning time of 3 days from a fluid-like to a better ordered gel structure, as indicated by the appearance of two sharper rings. (c)  $\text{K}_2\text{CO}_3$  provides a 43.2% RH environment. Structural changes were already observed well within the time of a measurement. (d) NaCl provides 75.5% RH environment. At this humidity the structure changed drastically over the time of a measurement and Bragg spots due to the formation of crystalline domains were observed. All subsequent measurements were taken at 11.3% where membrane structure was most stable over time.

For a quantitative analysis, data were integrated over circles in reciprocal space ( $q_z, q_{||}$ ) and displayed as a 1-dimensional intensity profile, as shown in Fig. 4(c)–(e). In order to isolate the plasma membrane signal, the integrated buffer profile was subtracted from the integrated profile of the plasma membrane. A typical result is shown in Fig. 4(e) and shows a number of well developed correlation peaks that can be assigned to different molecular components, as will be discussed below.

To study the dependence of membrane structure on relative humidity, plasma membrane samples were scanned at four different humidities, 11.3%, 23.1%, 43.2% and 75.5% for times varying from 3 to 10 days. The corresponding X-ray data are shown in Fig. 5.

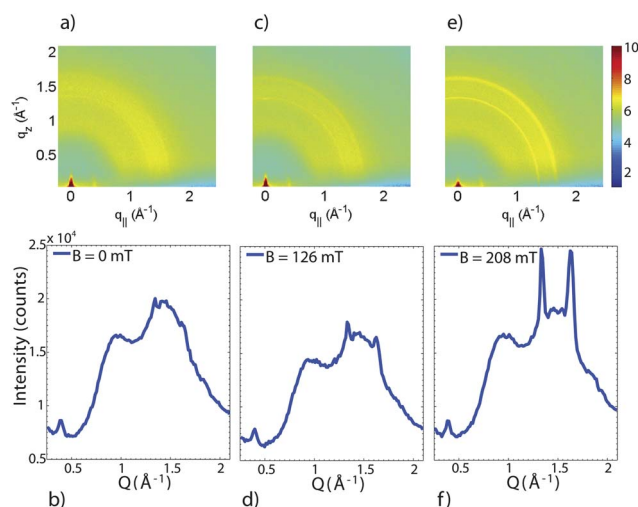


**Fig. 6** Two-dimensional and integrated diffracted intensities of plasma membrane in buffer with (a and b) no magnet, (c and d) 1 magnet and (e and f) 2 magnets. The plasma membrane scans show additional narrow and intense features in the presence of a magnetic field.

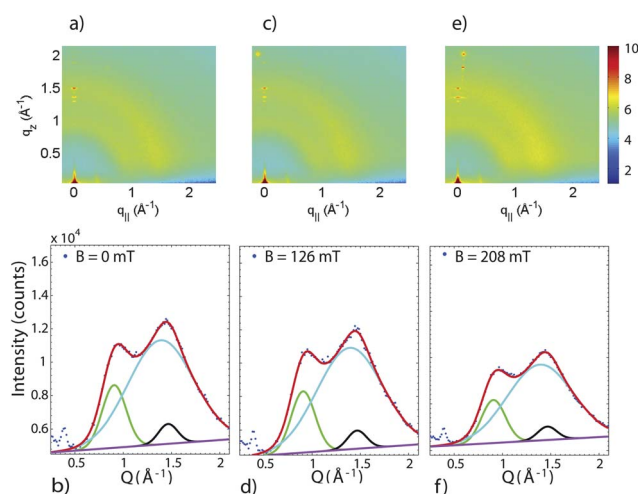


**Fig. 7** Two-dimensional and integrated diffracted intensities of buffer with (a and b) no magnet, (c and d) 1 magnet and (e and f) 2 magnets. The signals were fit by three Gaussian peak profiles. The peak intensities slightly decrease with increasing magnetic field.

The scans in Fig. 5 show the typical isotropic scattering intensities seen as semi-circular bands. While the intensity at the low relative humidity of 11.3% RH in Fig. 5(a) is very diffuse, sharper bands become visible at higher humidities. After equilibrating for several days at 75.5% in Fig. 5(d), well defined and bright spot-like intensities appear. The diffuse intensity is the signature of a disordered membrane structure. We assigned the sharp bands to a better ordered gel state of the plasma membranes. Bright, spot-like intensities are indicative of well-ordered, crystal-like membrane patches.

Some qualitative conclusions can be drawn from the measurements in Fig. 5: the time series of 11.3% RH, in Fig. 5(a), shows no change of the pattern over a timescale of

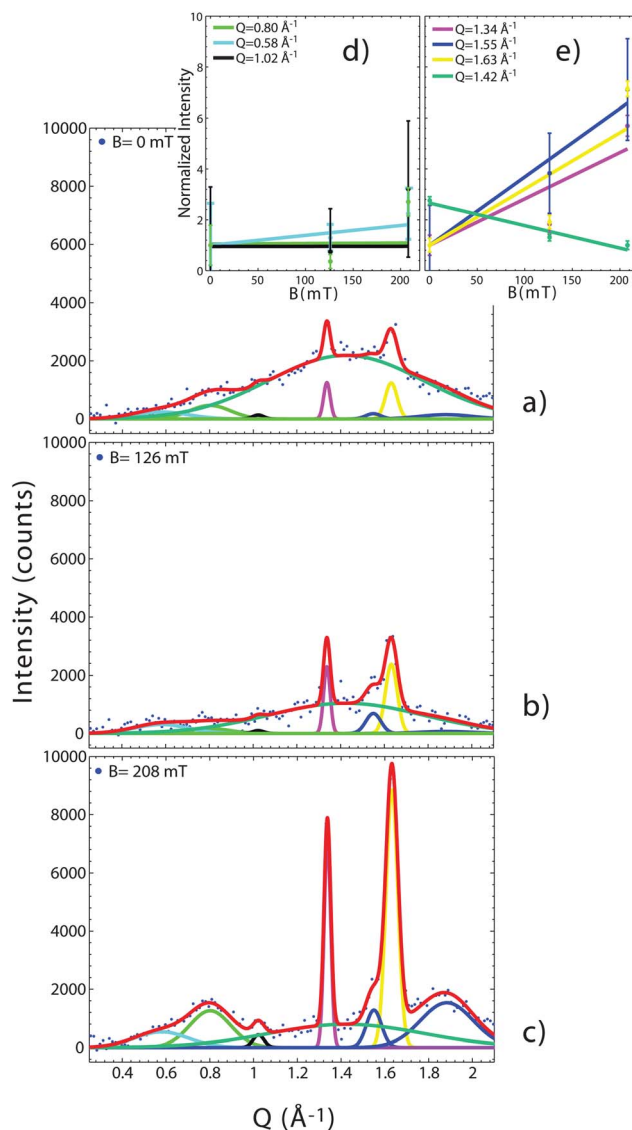


**Fig. 8** Fits of the integrated 2-dimensional X-ray scattering data of plasma membrane for each of the different magnetic field exposures (a) 0 mT, (b) 126 mT, and (c) 208 mT. The corresponding buffer scans were subtracted. Peak areas as determined from the fits as function of magnetic field strength are depicted in (d) and (e). The integrated intensities were normalized to the peak areas at zero magnetic field for easy comparison. Lines shown are guides for the eye. Error bars represent  $\sigma$  deviation.

**Table 3** Position, width and integrated intensities as determined by fits of Gaussian peak profiles to the correlation peaks in the data in Fig. 8

Gaussian		Peak position $Q$ ( $\text{\AA}^{-1}$ )	Peak width $\Delta Q$ ( $\text{\AA}^{-1}$ )	Integrated intensity (counts $\times \text{\AA}^{-1}$ )		
				$B = 0$ T	$B = 0.126$ T	$B = 0.208$ T
1	Protein component	0.58	0.28	93.1	93.1	163.7
2		0.80	0.20	163.0	59.1	293.6
3		1.02	0.09	39.4	14.3	27.2
4	Fluid lipid component	1.42	0.75	1713.2	843.1	704.5
5	Gel lipid component	1.34	0.04	46.5	91.9	270.3
6		1.55	0.06	13.2	49.5	110.9
7		1.63	0.06	82.4	159.0	602.5
8	Water component	1.88	0.30	150.6	55.8	461.3

several days. After 6 days at 75.5% RH, bright spots were visible in Fig. 5(d) indicating a very well ordered, crystalline structure. The general trend is that the higher the humidity, the faster the membrane structure changed from fluid-like into ordered gel-like structures. We chose, therefore, the low humidity state at 11.3% RH to study the effect of magnetic fields on molecular membrane structure.

To study the effect of magnetic fields on the structure of plasma membrane, samples consisting of only membrane buffer and plasma membrane samples including buffer were exposed to magnetic fields, and their 2-dimensional diffraction patterns measured. The 2-dimensional data were integrated over circular arcs in order to obtain 1-dimensional (line) scans. Fig. 6 and 7 depict the integrated intensities of plasma membrane and buffer sample exposed to no magnet, one-magnet and two-magnets, corresponding to magnetic fields of 0 T, 0.126 T and 0.208 T, respectively.

To isolate the scattering contribution of the plasma membrane; *i.e.*, of the lipid and protein components, scattering of the buffer solution was subtracted from the total plasma membrane scattering. In order to eliminate potential effects of the magnetic field on the pure buffer solution, buffer was also measured at the different magnetic field strengths.

The subtracted data are shown in Fig. 8(a)–(c). Several pronounced correlation peaks are visible. While a broad scattering contribution was dominant at zero magnetic field, as shown in Fig. 8(a), the broad component significantly lost intensity at high magnetic fields in favour of several narrow components, Fig. 8(c).

The correlation peaks in Fig. 8(a)–(c) were well fit using 8 Gaussian peak profiles. Position, width (FWHM) and integrated intensity of the peaks are given in Table 3 for the different magnetic field strengths. Fig. 8(d) and (e) depict the integrated peak intensities as function of magnetic field strength.

## Discussion

The lipid component of plant plasma membrane consists of three major classes of lipids: glycerolipids (mainly phospholipids), sterols and sphingolipids.<sup>23</sup> The most abundant lipid species are referred to as “structural lipids” up to 80% of which are phosphocholine (PC) and phosphoethanolamine (PE) phospholipids. The correlation peaks observed in the data in

Fig. 8 at  $1.34 \text{\AA}^{-1}$ ,  $1.55 \text{\AA}^{-1}$  and  $1.63 \text{\AA}^{-1}$  (‘5’, ‘6’, ‘7’) including the broad peak centred at  $1.42 \text{\AA}^{-1}$  (‘4’) (see also Table 3) can be assigned to the lipid component of the plasma membrane.

The position and width of the broad component agrees well with correlation peaks reported from single and multi-component phospholipid fluid lipid membranes.<sup>24–32</sup> This broad correlation peak is the tell-tale sign of a fluid, disordered membrane structure. The average nearest-neighbour distance between two lipid tails can be calculated from the peak position to  $\sim 5.1 \text{\AA}$  (for hexagonally-packed tails, the nearest-neighbour distance is  $4\pi/\sqrt{3} \cdot 1/(q_T)$ ). We note that the X-ray data in Fig. 6 agree well with X-ray data published by Welte *et al.*<sup>33</sup>

The narrow components in Fig. 8(a–c) are in good agreement with structural features reported in lipid membranes in their well ordered gel phase, where the lipid tails take an all-*trans* conformation. A correlation peak at  $\sim 1.5 \text{\AA}^{-1}$  was found in the gel phase of saturated phospholipid membranes, such as DMPC (dimyristoyl-*sn*-glycero-3-phosphocholine) and DPPC (dipalmitoyl-*sn*-glycero-3-phosphocholine).<sup>27,34,35</sup> Unsaturated lipids were reported to order in a structure with slightly larger nearest neighbour tail distances, leading to an acyl-chain correlation peak at  $\sim 1.3 \text{\AA}^{-1}$ , as reported for DOPC and POPC,<sup>36</sup> for instance. Lipids, such as dimyristoylphosphatidylethanolamine (DMPE) and the charged DMPS (dimyristoyl-*sn*-glycero-3-phosphoserine) with smaller head groups were reported to order in more densely packed structures.<sup>37</sup> The corresponding acyl chain correlation peaks were observed at  $Q$  values of  $Q \sim 1.65 \text{\AA}^{-1}$ . Because of the good agreement between the  $Q$ -positions reported in the literature and the positions in Table 3, we assigned the correlation peaks in Table 3 at  $Q$ -values of  $1.34 \text{\AA}^{-1} < Q < 1.63 \text{\AA}^{-1}$  to the lipid component of the plasma membranes. The fluidity of the membranes, *i.e.* the ratio between lipids in their fluid and gel state, can be estimated by the ratio of integrated intensities of the fluid peak (‘4’) in comparison to the gel-phase peaks (‘5’, ‘6’ and ‘7’).

The presence of the protein component in the plasma membrane led to additional scattering contributions. These proteins include receptor kinases, G-proteins, calcium signaling proteins and other cell-wall-related proteins.<sup>23</sup> We note that this experiment is not directly comparable to protein crystallography, where atomic resolution protein structure is determined from protein crystals. The proteins in our experiment are embedded in the plasma membrane, in a more natural state. The

corresponding structure is inherently disordered and shows the fingerprint of a dynamic, fluid-like state. While long-range order is absent, short-range correlations due to internal protein structure lead to the correlation peaks that we observe in Fig. 8.

Helical diffraction patterns related to structure and organization of  $\alpha$ -helices present in plasma and cell membranes were reported previously by, *e.g.* refs. 31 and 38–41. The diffraction pattern of an ideal helix was first written down by Pauling and Corey.<sup>42</sup> The pitch,  $P$ , and the radius,  $R_h$ , of the  $\alpha$ -helix give rise to the so-called helix peaks at  $Q$  values of  $2\pi/P$  and  $5\pi/8R_h$ . These peaks are observed in the data in Fig. 8. We tentatively assigned the corresponding maxima at  $Q$ -values of  $Q = 0.58 \text{ \AA}^{-1}$  (peak '3') and  $Q = 1.02 \text{ \AA}^{-1}$  (peak '5') to the helix peaks related to pitch and radius of the coils. The corresponding values for  $R_h$  and  $P$  were found to be  $R_h \sim 3.4 \text{ \AA}$  and  $P \sim 6.14 \text{ \AA}$ . The width of the peaks indicates a certain distribution of these parameters. Using the values given in Table 3,  $R_h = 3.39 \pm 0.7 \text{ \AA}$  and  $P = 6.14 \pm 0.39 \text{ \AA}$  are determined. This distribution is most likely the result of fluctuations of the helical structures and different compositions and molecular components.

The organization of  $\alpha$ -helices inside of the helical domains of proteins was reported to give rise to additional scattering maxima. These peaks are related to nearest neighbour distances of the helices, as discussed in for instance, refs. 38 and 40. We tentatively assigned the correlation peaks at  $Q$ -values of  $Q = 0.80 \text{ \AA}^{-1}$  to the organization of  $\alpha$ -helices inside the helical domains of the plant plasma membrane proteins. The corresponding distance was calculated to be  $7.9 \text{ \AA}$  ( $= 2\pi/0.8 \text{ \AA}^{-1}$ ). This value is slightly larger than the diameter of the coils ( $2 \times R_h = 6.8 \text{ \AA}$ ), which indicates a densely packed helical structure, as can be expected.

A correlation peak in lipid membranes located at  $Q \sim 1.88 \text{ \AA}^{-1}$  was previously assigned to the nearest neighbour distance between hydration water molecules.<sup>19,28,43–45</sup> While the distance between water molecules in bulk water is observed at  $\sim 3.14 \text{ \AA}$  (corresponding to a  $Q$ -value of  $2 \text{ \AA}^{-1}$ ), hydration water molecules were found to have a slightly larger nearest neighbour distance of  $\sim 3.4 \text{ \AA}$ . Correlation peak '8' in Table 3 was, therefore assigned to hydration water molecules.

As listed in Table 3, the assignment of the correlation peaks observed in Fig. 8(a)–(c) can be summarized as follows: scattering intensities at  $Q$ -values  $Q \leq 1 \text{ \AA}^{-1}$  were assigned to inter- and intra-protein structures of the plant plasma membrane proteins related to helical structures and alignment in the helical domains of the proteins. Peaks at intermediate  $Q$ -values  $1 \text{ \AA}^{-1} \leq Q \leq 1.65 \text{ \AA}^{-1}$  agree well with gel and fluid lipid structures reported in the literature and were, therefore, assigned to the lipid component of the plasma membranes. The scattering intensity at  $Q \sim 1.88 \text{ \AA}^{-1}$  was assigned to the nearest neighbour distance of hydration water molecules. The assignments of correlation peaks to molecular components are also depicted in Fig. 9.

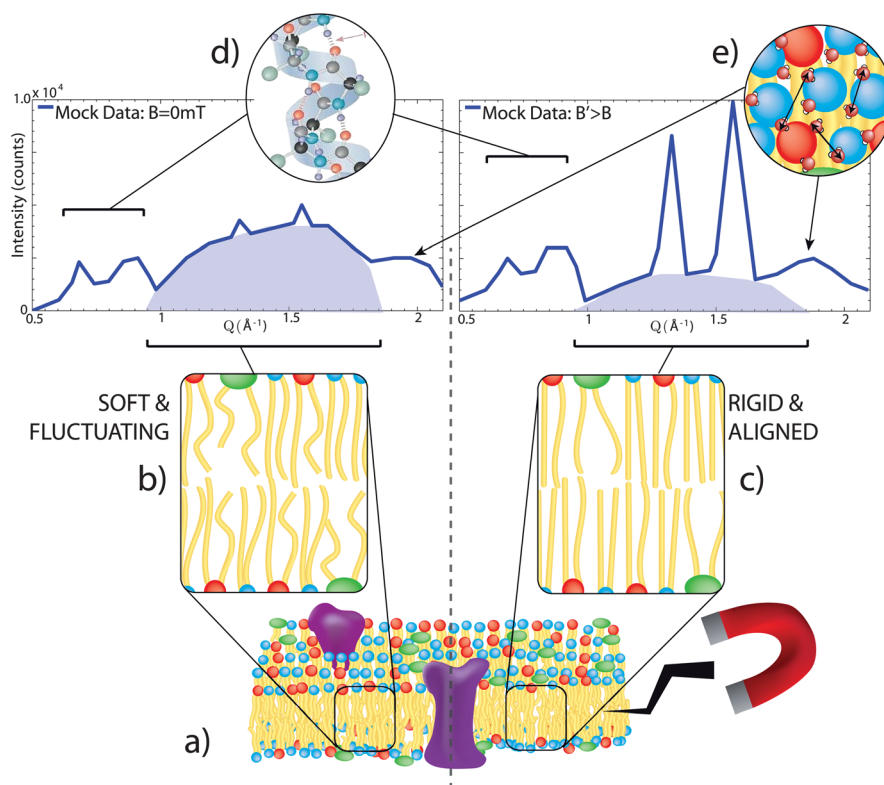
The presence of an external magnetic field led to significant structural changes in the plasma membrane, as observed in the data in Fig. 8(b) and (c): while the broad fluid membrane component decreases, the intensities of the correlation peaks assigned to the gel lipid component of the membrane (peaks '5', '6' and '7' in Table 3) significantly increased in intensity.

Fig. 8(d) and (e) show the integrated intensities for all peaks as function of the external magnetic field. Peak areas were normalized to the peak area in non applied magnetic field for an easy comparison (with the exception of peak '4', which is normalized to the peak area for 208 mT field to emphasize the negative slope); absolute values for the integrated peak intensities are listed in Table 3. While the intensities of the protein peaks did not change systematically within the resolution and statistics of this experiment, the area of the peak assigned to the fluid component of the lipid component decreased by a factor of three to  $\sim 35\%$  while the gel component significantly increased by  $\sim 600\%$ . The observed changes are well outside of the (conservative) experimental error bars. The increase of the correlation peaks of the well ordered gel phase, and, at the same time, loss of intensity in the fluid peak indicates an increased order in the lipid component of the plant plasma membrane in the presence of static magnetic fields. We also note an increase in the intensity of the water correlation peak with increasing magnetic field.

Because the magnetic fields in this experiment were achieved by permanent magnets, it was not possible to change the magnetic field strength *in situ*. We can, therefore, at this point not comment on the reversibility of the magnetic field effects, *i.e.*, if the structure returned to its initial state if the magnetic field was switched off. This information would be important in understanding if the effect of the field is to facilitate the kinetics of a transition (from a disordered to an ordered lipid phase) that is slow in the absence of the field, or if the field is moving the system to a new equilibrium state.

To the best of our knowledge very few studies investigated molecular order in native plasma membranes using X-ray or neutron diffraction techniques, most likely due to the underlying experimental challenges. Our results can be compared to the work by Engelman,<sup>46</sup> Welte *et al.*<sup>33</sup> and Esfahani *et al.*<sup>47</sup> The corresponding wide angle X-ray diffraction patterns agree well with the data in this paper: a broad, diffuse intensity at  $\sim 4.5 \text{ \AA}$  (corresponding to a  $Q$ -value of  $\sim 1.4 \text{ \AA}^{-1}$ ) was observed and assigned to the fluid state of the closely packed lipid acyl-chains. A sharp and pronounced intensity line at  $\sim 4.2 \text{ \AA}$  (corresponding to a  $Q$ -value of  $\sim 1.5 \text{ \AA}^{-1}$ ) was assigned to lipid tails in their well ordered gel phase. We note that the data presented in Fig. 5–7 show significantly more details than the diffraction patterns published decades ago due to advances in scattering equipment. The unprecedented intensity and resolution enabled us for the first time to assign the observed intensities to various membrane components, such as different lipid species and helical protein structures. Also, structural changes due to hydration of the membranes and in particular exposure to external magnetic fields could be studied and their impact on membrane structure quantified.

The exact mechanism of the interaction between magnetic fields and seeds is not yet known, despite the extensive reports of pronounced seed performance after magnetic field exposure.<sup>9–11</sup> Some findings of this study (summarized in Fig. 9) add to the debate about the probable mechanisms, strongly pointing to the seed plasma membrane as a likely target site for magnetic field interaction. First, because higher magnetically



**Fig. 9** Assignment of the correlation peaks to molecular components of a native plant plasma membrane. (a) Schematic of plant plasma membrane including lipid and protein component. (b) The range  $1 \text{ \AA}^{-1} \leq Q \leq 1.65 \text{ \AA}^{-1}$  was assigned to the lipid component. (c) In the presence of a magnetic field the lipid tails transform into an all-*trans* configuration. (d) Signals at  $0.5 \text{ \AA}^{-1} \leq Q \leq 1 \text{ \AA}^{-1}$  were assigned to  $\alpha$ -helical protein structures. The intensity of these peaks are unchanged with respect to increased magnetic field strength within the error of our experiment. (e) Hydration water bound to lipid head groups was assigned to the correlation peak at  $Q = 1.88 \text{ \AA}^{-1}$ . The  $\alpha$ -helix representation is a work of the National Institutes of Health.

induced ordering in lipids can be regarded as a local change in the physical properties of lipid bilayers, this physical change could induce deformation in the plasma membrane and ease vesicle fusion or budding.<sup>23</sup> Second, because plasma membrane lipids critically influence cell structures, membrane fluidity as well as signal transduction,<sup>23</sup> membrane lipid ordering under static magnetic field exposure could lead to reduced membrane lipid fluidity due to their inverse relationship.<sup>48</sup>

Reduced plasma membrane fluidity could explain the reduced electrolytes leakage in magnetically treated seeds such as tomato and chickpeas during early water uptake in the seed germination process.<sup>12</sup> Although we have some direct evidence that a static magnetic field influences lipid membrane order, several uncertainties remain. Because the plasma membrane purification process yields approximately 40–50% inside-out vesicles,<sup>13</sup> the dependency of the observed effects on sidedness of the plasma membrane samples is unclear. In addition, systematic constraints have limited this study to south field exposure, and any relationship of magnetic field polarity on the plasma membrane cannot be excluded so far. Additionally, since the plasma membrane represents approximately 5–20% of the total membranes in a plant cell<sup>13</sup> and the plasma membrane was taken outside the mature seeds for the purpose of the current study, it remains to be demonstrated how changes at membrane level in intact mature seeds exposed to static

magnetic fields would affect their resulting performance, considering that biological membranes are thought to be discrete, ordered islands rather than uniform bilayers containing lipids and proteins.<sup>23,49</sup>

## Conclusions

In summary, we studied effects of external static magnetic fields on purified tomato seed plasma membranes mounted on a silicon substrate. We measured the changes in the molecular structure as a function of magnetic field strength using X-ray diffraction measurements. The molecular structure of plant plasma membranes was found to strongly depend on the relative humidity. At relative humidities greater than 11.3% RH, the membranes were found to be transformed into highly ordered gel structures on timescales shorter than an X-ray measurement of 27 hours. Membrane samples were, therefore, measured at a low relative humidity of 11.3% RH.

Correlation peaks were observed in the X-ray diffraction data, which were assigned to the protein, the lipid and the water components of the plasma membranes. Peaks related to the protein component were assigned to  $\alpha$ -helix dimensions, helix radius and pitch, as well as the ordering of helices in the helical domain of the proteins. Four correlation peaks were assigned to gel and fluid structures of different lipid classes that generally

occur in plasma membranes. With an applied external magnetic field, a significant increase of the gel lipid component was observed. At the same time the fluid component decreased. There was no significant structural change to the protein structure with increasing magnetic field within the resolution and statistics of this experiment. This leads us to the overall conclusion that external magnetic fields interact predominantly with the lipid component of plant plasma membrane and less with the membrane proteins.

## Acknowledgements

The authors wish to thank Tim Sutor (Heinz, Canada) for providing the seeds, Dr Joanna Porankiewicz-Asplund (Agrisera, Sweden) for providing the antibodies. Funding was provided by the Canadian Commonwealth Scholarship Program (CCSP) and the Mauritius Research Council (MRC) postgraduate award to D.P. This research was also funded by the Natural Sciences and Engineering Research Council of Canada (NSERC), the National Research Council Canada (NRC), the Canada Foundation for Innovation (CFI) and the Ontario Ministry of Economic Development and Innovation (OMEDI). M.C.R. is the recipient of an Early Researcher Award of the Province of Ontario.

## References

- 1 T. Ritz, P. Thalau, J. B. Phillips, R. Wiltschko and W. Wiltschko, *Nature*, 2004, **429**, 177.
- 2 S. Johnsen and K. J. Lohmann, *Nat. Rev. Neurosci.*, 2005, **6**, 703.
- 3 K. Maeda, K. B. Henbest, F. Cintolesi, I. Kuprov, C. T. Rodgers, P. A. Liddell, D. Gust, C. R. Timmel and P. J. Hore, *Nature*, 2008, **453**, 387.
- 4 C. D. Treiber, M. C. Salzer, J. Riegler, N. Edelman, C. Sugar, M. Breuss, P. Pichler, H. Cadiou, M. Saunders, M. Lythgoe, *et al.*, *Nature*, 2012, **484**, 367–370.
- 5 D. Faivre and D. Schüler, *Chem. Rev.*, 2008, **108**, 4875.
- 6 R. P. Blakemore, *Annu. Rev. Microbiol.*, 1982, **36**, 217.
- 7 M. V. Berry and A. K. Geim, *Eur. J. Phys.*, 1997, **18**, 307–313.
- 8 S. Pacini, M. Gulisano, B. Peruzzi, E. Sgambati, G. Gheri, S. Gheri Bryk, S. Vannucchi, G. Polli and M. Ruggiero, *Cancer Detect. Prev.*, 2003, **27**, 327.
- 9 N. Belyavskaya, *Adv. Space Res.*, 2004, **34**, 1566–1574.
- 10 P. Galland and A. Pazur, *J. Plant Res.*, 2005, **118**, 371.
- 11 S. Harris, K. Henbest, K. Maeda, J. Pannell, C. Timmel, P. Hore and H. Okamoto, *J. R. Soc., Interface*, 2009, **6**(41), 1193.
- 12 A. Vashisth and S. Nagarajan, *Bioelectromagnetics*, 2008, **29**, 571.
- 13 C. Larsson and S. Widell, *Methods Biotechnol.*, 2000, **11**, 159.
- 14 V. Santoni, *Methods Mol. Biol.*, 2006, **355**, 93.
- 15 E. Alexandersson, N. Gustavsson, K. Bernfur, A. Karlsson, P. Kjellbom and C. Larsson, *Methods Mol. Biol.*, 2008, **432**, 161.
- 16 M. Bradford, *Anal. Biochem.*, 1976, **72**, 248.
- 17 M. Nouri and S. Komatsu, *Proteomics*, 2010, **10**, 1930.
- 18 M. A. Barrett, S. Zheng, G. Roshankar, R. J. Alsop, R. K. Belanger, C. Huynh, N. Kučerka and M. C. Rheinstädter, *PLoS ONE*, 2012, **7**, e34357.
- 19 L. Toppozini, C. L. Armstrong, M. A. Barrett, S. Zheng, L. Luo, H. Nanda, V. G. Sakai and M. C. Rheinstädter, *Soft Matter*, 2012, **8**(47), 11839–11849.
- 20 G. Pabst, N. Kučerka, M.-P. Nieh, M. Rheinstädter and J. Katsaras, *Chem. Phys. Lipids*, 2010, **163**, 460.
- 21 M. C. Rheinstädter, Neutron scattering applications and techniques, *Lipid Membrane Dynamics*, Springer, US, 2012, pp. 263–286.
- 22 G. Fragneto and M. Rheinstädter, *C. R. Phys.*, 2007, **8**, 865.
- 23 F. Furt, F. Simon-Plas and S. Mongrand, Lipids of the Plant Plasma Membrane, *The Plant Plasma Membrane, vol. 19 of Plant Cell Monographs*, Springer, US, 2011, pp. 57–85.
- 24 N. Kučerka, Y. Liu, N. Chu, H. I. Petrache, S. Tristram-Nagle and J. F. Nagle, *Biophys. J.*, 2005, **88**, 2626.
- 25 H. I. Petrache, N. Gouliarov, S. Tristram-Nagle, R. Zhang, R. M. Suter and J. F. Nagle, *Phys. Rev. E: Stat. Phys., Plasmas, Fluids, Relat.*, 1998, **57**, 7014.
- 26 N. Kucerka, S. Tristram-Nagle and J. F. Nagle, *Biophysical Journal: Biophysical Letters*, 2006, **90**, L83.
- 27 M. C. Rheinstädter, C. Ollinger, G. Fragneto, F. Demmel and T. Salditt, *Phys. Rev. Lett.*, 2004, **93**, 108107.
- 28 M. C. Rheinstädter, T. Seydel and T. Salditt, *Phys. Rev. E: Stat. Phys., Plasmas, Fluids, Relat.*, 2007, **75**, 011907.
- 29 M. C. Rheinstädter, J. Das, E. J. Flenner, B. Brüning, T. Seydel and I. Kosztin, *Phys. Rev. Lett.*, 2008, **101**, 248106.
- 30 J. Pan, T. T. Mills, S. Tristram-Nagle and J. F. Nagle, *Phys. Rev. Lett.*, 2008, **100**, 198103.
- 31 P. Schneggenburger, A. Beerlink, B. Weinhausen, T. Salditt and U. Diederichsen, *Eur. Biophys. J.*, 2011, **40**, 417.
- 32 T. A. Harroun, W. T. Heller, T. M. Weiss, L. Yang and H. W. Huang, *Biophys. J.*, 1999, **76**, 937–945.
- 33 R. Welti, D. Rintoul, F. Goodsaid-Zalduondo, S. Felder and D. Silbert, *J. Biol. Chem.*, 1981, **256**, 7528.
- 34 S. Tristram-Nagle, Y. Liu, J. Legleiter and J. F. Nagle, *Biophys. J.*, 2002, **83**, 3324.
- 35 J. Katsaras, V. A. Raghunathan, E. J. Dufourc and J. Dufourcq, *Biochemistry*, 1995, **34**, 4684.
- 36 T. T. Mills, J. Huang, G. W. Feigenson and J. F. Nagle, *Gen. Physiol. Biophys.*, 2009, **28**, 126.
- 37 M. Rappolt and G. Rapp, *Ber. Bunsenges. Phys. Chem.*, 1996, **100**, 1153–1162.
- 38 A. Spaar, C. Münster and T. Salditt, *Biophys. J.*, 2004, **87**, 396.
- 39 T. Salditt, C. Li and A. Spaar, *Biochimica et Biophysica Acta (BBA) – Biomembranes*, 2006, **1758**, 1483.
- 40 D. S. Fudge, K. H. Gardner, V. T. Forsyth, C. Riekel and J. M. Gosline, *Biophys. J.*, 2003, **85**, 2015–2027.
- 41 S. Carito, S. Bazil and G. Digiacoimo, *J. Bacteriol.*, 1967, **93**, 122.
- 42 L. Pauling and R. B. Corey, *Proc. Natl. Acad. Sci. U. S. A.*, 1951, **37**, 235–240.
- 43 L. Toppozini, C. L. Armstrong, M. D. Kaye, M. Tyagi, T. Jenkins and M. C. Rheinstädter, *ISRN Biophys.*, 2012, **2012**, 520307.

- 44 M. C. Rheinstädter, T. Seydel, F. Demmel and T. Salditt, *Phys. Rev. E: Stat. Phys., Plasmas, Fluids, Relat.*, 2005, **71**, 061908.
- 45 A. M. Gaspar, S. Busch, M.-S. Appavou, W. Haeussler, R. Georgii, Y. Su and W. Doster, *Biochim. Biophys. Acta*, 2010, **1804**, 7682.
- 46 D. M. Engelman, *J. Mol. Biol.*, 1970, **47**, 115.
- 47 M. Esfahani, A. R. Limbrick, S. Knutton, T. T. Oka and S. J. Wakil, *Proc. Natl. Acad. Sci. U. S. A.*, 1971, **68**, 3180.
- 48 Y. Nakaoka, J. Itoh and K. Shimizu, *Bioelectromagnetics*, 2011, **32**, 66.
- 49 L. Rajendran and K. Simons, *J. Cell Sci.*, 2005, **118**, 1099.